Modulation of Convectively Coupled Kelvin Wave Activity in the Tropical Pacific by ENSO

WANG Hui[1,2]* (王　辉), PAN Yutong[3] (潘宇彤), Arun KUMAR[1], and WANG Wanqiu[1] (王万秋)

1 *NOAA/NWS/NCEP/Climate Prediction Center, College Park, MD 20740, USA*

2 *Wyle Science, Technology and Engineering Group, McLean, VA 22102, USA*

3 *Department of Atmospheric and Oceanic Science, University of Maryland, College Park, MD 20742, USA*

ABSTRACT

The influence of El Niño–Southern Oscillation (ENSO) on the convectively coupled Kelvin waves over the tropical Pacific is investigated by comparing the Kelvin wave activity in the eastern Pacific (EP) El Niño, central Pacific (CP) El Niño, and La Niña years, respectively, to 30-yr (1982–2011) mean statistics. The convectively coupled Kelvin waves in this study are represented by the two leading modes of empirical orthogonal function (EOF) of 2–25-day band-pass filtered daily outgoing longwave radiation (OLR), with the estimated zonal wavenumber of 3 or 4, period of 8 days, and eastward propagating speed of 17 m s^{-1}. The most significant impact of ENSO on the Kelvin wave activity is the intensification of the Kelvin waves during the EP El Niños. The impact of La Niña on the reduction of the Kelvin wave intensity is relatively weaker, reflecting the nonlinearity of tropical deep convection and the associated Kelvin waves in response to ENSO sea surface temperature (SST) anomalies. The impact of the CP El Niño on the Kelvin waves is less significant due to relatively weaker SST anomalies and smaller spatial coverage. ENSO may also alter the frequency, wavelength, and phase speed of the Kelvin waves. This study demonstrates that low-frequency ENSO SST anomalies modulate high-frequency tropical disturbances, an example of weather-climate linkage.

Key words: convectively coupled Kelvin waves, El Niño–Southern Oscillation (ENSO), outgoing longwave radiation (OLR), empirical orthogonal function (EOF), power spectra

1. Introduction

Convectively coupled Kelvin waves are equatorially-trapped waves that are well organized along with anomalous deep convection and propagate eastward (Wheeler and Kiladis, 1999). They interact with a range of important weather-climate systems in the tropics, including the Madden-Julian Oscillation (MJO) over the tropical Indian Ocean (Roundy, 2008), the intertropical convergence zone (ITCZ) in the tropical Pacific and Atlantic regions (Dias and Pauluis 2011; Wang and Fu, 2007), the South American monsoon (Liebmann et al., 2009), and the West African monsoon (Mounier et al., 2008).

Since deep convection anomalies are embedded in the Kelvin waves, the underlying tropical sea surface temperature (SST) that strongly controls deep convection may also alter the characteristics of the Kelvin waves. Figure 1 shows two examples of anomalous deep convection during 1982/83 El Niño and 2005/06 La Niña represented by 2–25-day band-pass filtered daily outgoing longwave radiation (OLR; Liebmann and Smith, 1996; see Section 2 for data details) at the equator. In January 1983 (Fig. 1a), very active convective disturbances existed across the tropical Pacific, consistent with the warmer SST associated with El Niño. Some disturbances were well organized and propagated eastward. In January 2006 (Fig. 1b), convection and the related wave activity were largely suppressed in the central and eastern equatorial Paci-
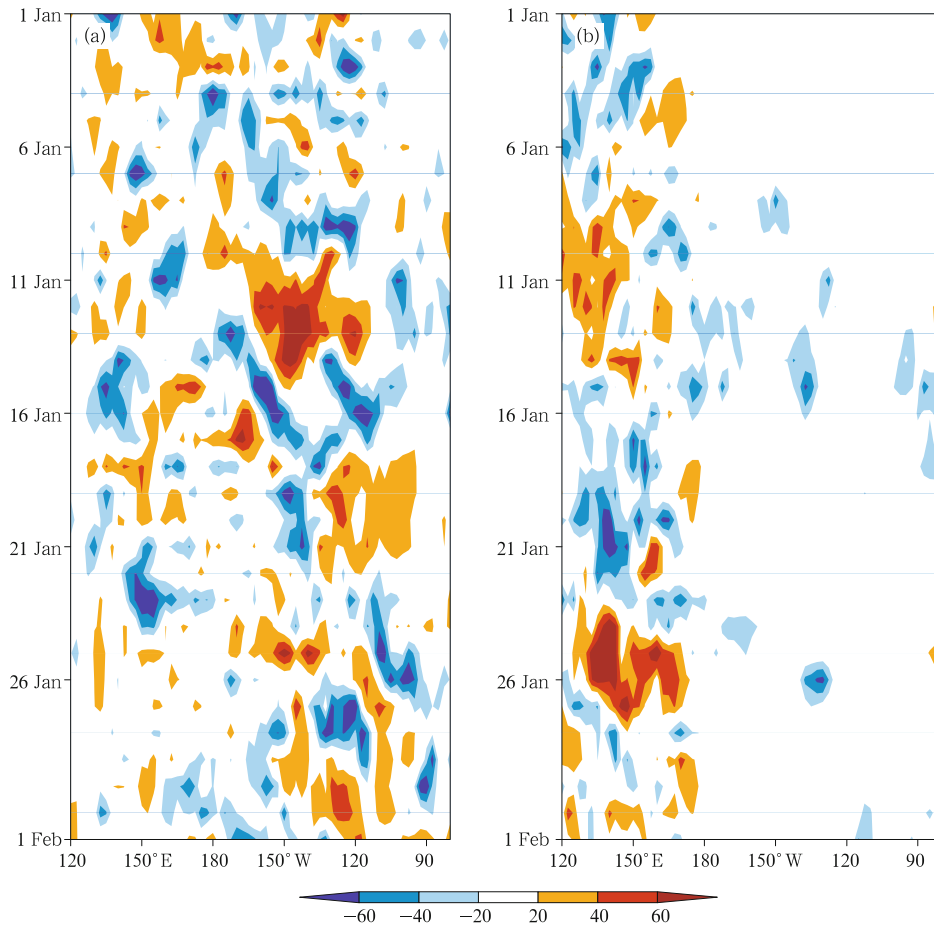
Fig. 1. Longitude-time diagram of band-pass (2–25-day) filtered daily OLR (W m^{-2}) at the equator in (a) January 1983 and (b) January 2006.

fic due to colder La Niña SST. Figure 1 indicates a significant influence of El Niño–Southern Oscillation (ENSO) on the tropical deep convection and the associated wave activity.

Given the slow-varying SST associated with ENSO, its modulation of the daily convection shown in Fig. 1 suggests a possible low-frequency SST influence on high-frequency tropical disturbances, including the Kelvin waves on a sub-monthly timescale. The subject is of particular interest when we view weather and climate as a continuum spanning all timescales. The intensity and frequency of occurrence of different ENSO flavors have changed over decades and may continue to change in the future (e.g., Kim and Yu, 2012). We expect that the ENSO modulation of the high-frequency tropical disturbances and Kelvin waves also change with time. Because the convectively cou-

pled Kelvin waves interact with some important tropical weather-climate systems, a better understanding of the ENSO modulation of the Kelvin waves will also help understand and anticipate the changes in the impact of ENSO on these systems in a changing climate.

The purpose of this study is to explore possible modulations of convectively coupled Kelvin waves by ENSO. In particular, we will examine how El Niño and La Niña affect the characteristics of the Kelvin waves, including intensity, frequency, wavelength, and phase speed. El Niño in this study is classified as the conventional eastern Pacific (EP) El Niño and central Pacific (CP) El Niño (Yeh et al., 2009). The latter, also called El Niño Modoki (Ashok et al., 2007), is shown to have occurred more frequently in recent 20 years (Kao and Yu, 2009) and caused a tropical precipitation pattern and thus deep convection different from EP El Niño

(e.g., Wang et al., 2012).

This paper is organized as follows. Section 2 provides a brief description of data and analysis methods. Section 3 characterizes convectively coupled Kelvin waves over the tropical Pacific and assesses the impacts of ENSO on the Kelvin wave activity associated with EP and CP El Niño, as well as La Niña. Conclusions are given in Section 4.

2. Data and methods

The datasets used in this study consist of National Oceanic and Atmospheric Administration (NOAA) Interpolated OLR (Liebmann and Smith, 1996), NOAA Optimum Interpolation SST version 2 (OISST v2; Reynolds et al., 2002), and National Centers for Environmental Prediction (NCEP)-Department of Energy (DOE) Reanalysis 2 (R2; Kanamitsu et al., 2002).

The OLR data are twice-daily satellite measurements and are interpolated into daily values on a 2.5°×2.5° (latitude×longitude) grid (Liebmann and Smith, 1996). The SSTs are monthly mean data on a 1°×1° grid. Daily 200-hPa divergent winds are derived from daily 200-hPa zonal and meridional winds in R2 on a 2.5°×2.5° grid. All data cover the 30-yr period from January 1982 to December 2011 (10957 days).

Many previous studies of tropical waves use OLR to represent tropical deep convection (e.g., Wheeler and Kiladis, 1999; Roundy and Frank, 2004; Laing et al., 2011). Similar to Wang and Fu (2007) to identify the convectively coupled Kelvin waves over the tropical Atlantic, we apply the conventional empirical orthogonal function (EOF) method to daily OLR over the tropical Pacific. Prior to the EOF analysis, a Lanczos band-pass (2–25-day) filter (Duchon, 1979) is applied to the daily OLR data to highlight synoptic-scale and high-frequency signals and also eliminate day-to-day fluctuations, intraseasonal and longer timescale variations. As we will show in this paper, the two leading EOF modes of OLR capture the eastward propagating Kelvin waves that are coupled with deep convection across the tropical Pacific.

Three statistical methods are used to document the spatial structure of the Kelvin waves and the as-

sociated atmospheric dynamical fields, as well as wave characteristics. The first one is the correlative analysis, in which a temporal correlation coefficient is calculated between OLR and the principal component (PC) time series associated with the EOFs. Composites based on linear regressions against the PC time series are used to obtain the 200-hPa divergent wind pattern associated with the Kelvin waves. The third method is the power spectrum analysis, which is used to characterize the frequency or period of the Kelvin waves. The analysis is applied to each 365-day segment. The mean power spectra are the averages of individual 365-day spectra over selected years.

During the 30-yr period (1982–2011), there were 5 EP El Niño (1982/83, 1986/87, 1991/92, 1997/98, and 2006/07), 5 CP El Niño (1987/88, 1994/95, 2002/03, 2004/05, and 2009/10), and 8 La Niña (1983/84, 1984/85, 1988/89, 1995/96, 1998/99, 1999/2000, 2005/06, and 2007/08) events. Composites of the Kelvin wave activity for each ENSO category are derived and compared to the 30-yr mean statistics to illustrate the impact of ENSO. Because ENSO has a phase-locking behavior with respect to the annual cycle (Neelin et al., 2000), with the peak phase in boreal winter, we define an annual march based on the ENSO cycle starting from 1 June of a year to 31 May of next year.

3. Results

3.1 Convectively coupled Kelvin waves over the tropical Pacific

Figure 2 shows the spatial patterns of the first two EOFs of the 30-yr filtered (2–25-day band-pass) daily OLR in the tropical Pacific domain (10°S–10°N, 120°E–80°W). The spatial patterns are represented by the maps of correlation coefficients between the filtered OLR anomalies at each grid point and the PC time series of the two EOFs. Given the large size of samples (10957 days), the correlation values of ±0.05 are well above the 99% significance level estimated by the Monte Carlo test (e.g., Wilks, 1995).

Both EOFs display a well-defined wave pattern, which is characterized by two centers of negative correlations separated by a center of positive correlations
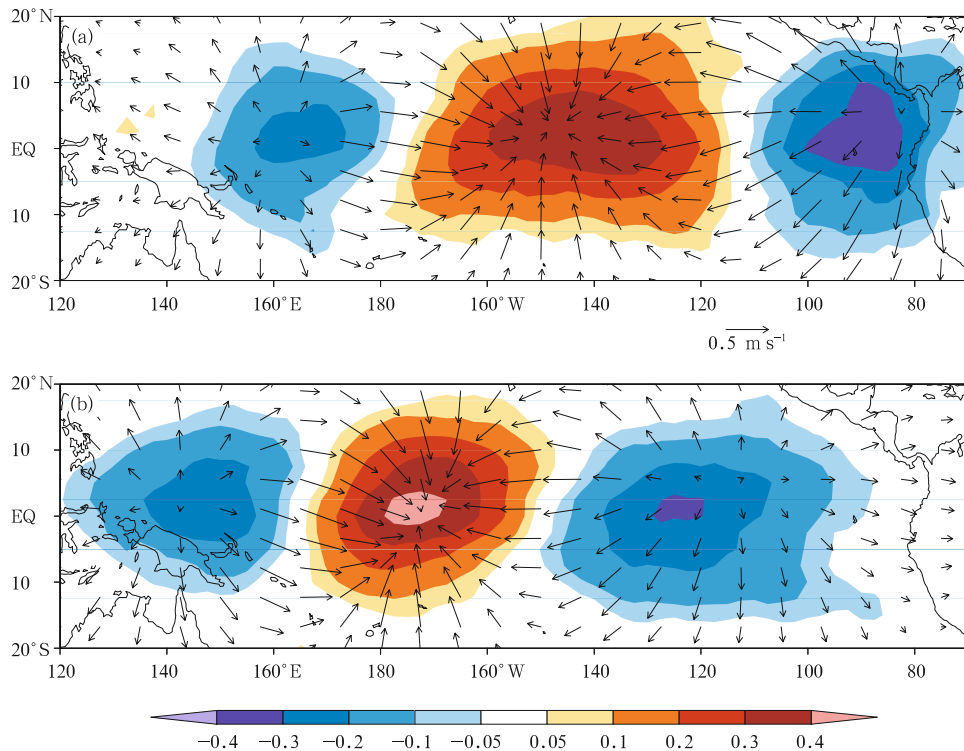
Fig. 2. Spatial patterns of the (a) first and (b) second EOFs of band-pass filtered daily OLR from 1 January 1982 to 31 December 2011. The maps are shown in the form of correlation coefficients (shadings) between filtered OLR anomalies and the PC time series associated with each EOF. Regression patterns of unfiltered daily 200-hPa divergent wind anomalies (vectors; m s^{-1}) associated with 1σ departure in the PC time series are superimposed.

along the equator over the tropical Pacific. The meridional locations of these centers slightly shift towards the north of the equator, likely related to the mean position of the ITCZ. The tripole structure suggests that weaker convection in the central Pacific tends to be associated with stronger convection in the western and eastern Pacific, and vice versa. Together the two modes account for 15% of filtered daily OLR variance over the equatorial Pacific. They are also distinct and well separated from the rest of the modes based on the rule of thumb suggested by North et al. (1982).

Superimposed onto the two EOF patterns of OLR are the 200-hPa divergent wind anomalies obtained by regressing unfiltered daily 200-hPa divergent wind anomalies against the corresponding PC time series. Upper-level outflows originate from the centers of negative correlations (enhanced convection) and inflows converge to the centers of positive correlations (weakened convection) associated with the two EOFs. Therefore, the two leading modes of OLR that repre-

sent the high-frequency variability of deep convection in the tropical Pacific are dynamically consistent with the upper-level circulation.

The two wave patterns in Fig. 2 are spatially orthogonal to each other due to the constraint of orthogonality for the EOF analysis. However, they have similar wavelengths, albeit with a phase shift. The wavelength is relatively short in the western Pacific (about 90° in longitude, zonal wavenumber 4) and relatively long in the eastern Pacific (about 120° in longitude, zonal wavenumber 3). The phase difference between the two waves is about 20°–30° in longitude.

In addition to the spatial orthogonality of the two EOFs, the two PCs are also temporally orthogonal with no correlation. However, lead and lag correlations between the two PCs are nonzero, as shown in Fig. 3. The correlation is highly significant when PC1 leads PC2 1–2 days (negative correlation) or lags 1–2 days (positive correlation). The peak correlations with lags of ±2 days suggest that both PC1 and PC2
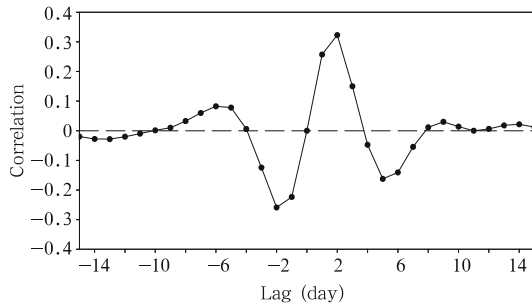
Fig. 3. Lag correlations between the two PC time series of the 30-yr daily OLR from day –15 (PC1 leading PC2 15 days) to day 15 (PC1 lagging PC2 15 days).

may oscillate with a period of 8 days. Figure 3 also indicates that peak convection associated EOF1 (Fig. 2a), for example, at the equator near 90°W, lags peak convection near 120°W associated with EOF2 (Fig.

2b) by 2 days, suggesting possible eastward propagation of convective disturbances.

Figure 4 shows an example of how the two leading EOFs represent the eastward propagating tropical convection along the equator in June 1992. The filtered (2–25-day band-pass) daily OLR anomalies (Fig. 4a) indicate a series of eastward propagating disturbances across the tropical Pacific during that month, as well as some westward propagating anomalies in the middle of the month. The reconstructed OLR anomalies (Fig. 4b) based on the two EOFs well capture the eastward propagating signals with no significant projection of the westward moving convection onto the two modes.

The eastward propagation of convective disturbances can be seen more clearly in the lead and lag
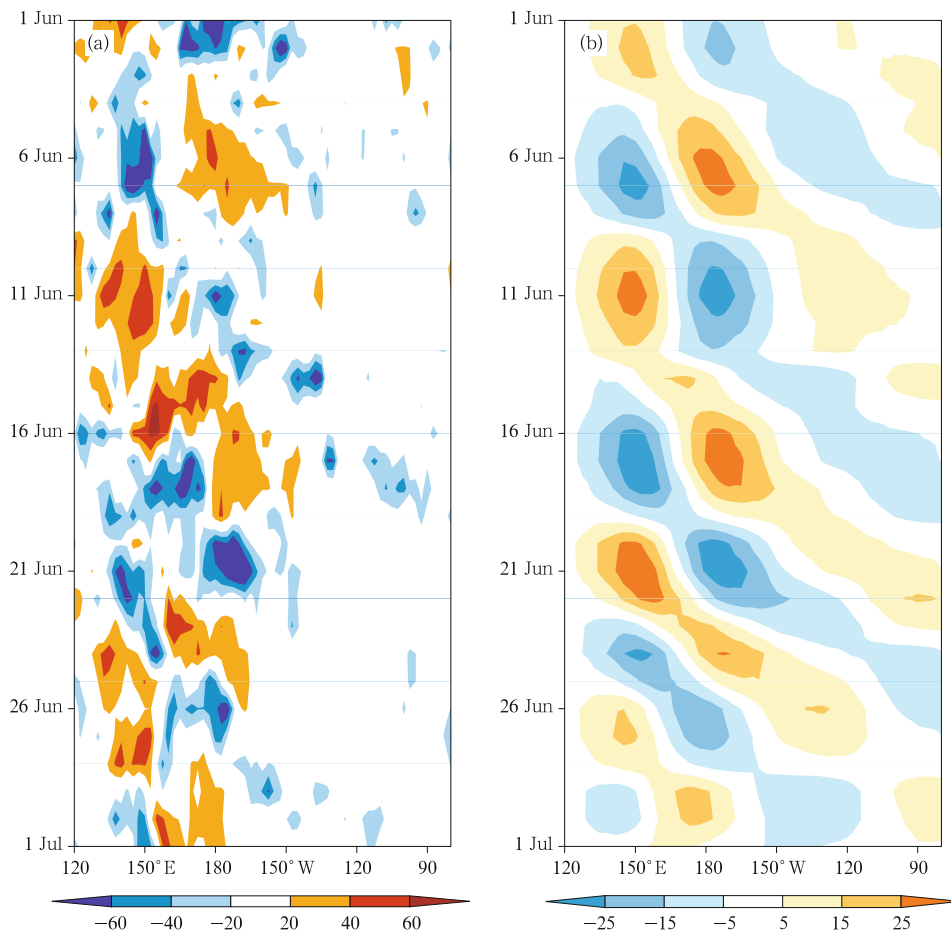
Fig. 4. Longitude-time diagrams of (a) band-pass (2–25-day) filtered daily OLR (W m^{-2}) at the equator in June 1992 and (b) corresponding reconstructed OLR anomalies based on the two leading EOFs.

correlation maps of OLR with PC1 and PC2 shown in Fig. 5, together with 200-hPa divergent wind anomalies obtained based on lead and lag linear regressions versus the two PC time series. As shown in Fig. 3, the two PCs are significantly correlated when PC1 leads PC2 by 1 and 2 days. Therefore, the spatial patterns shown in Fig. 5 are constructed based on those associated with the individual PCs in the following manner: 0.5PC1+0.25[PC2(t+1)+PC2(t+2)], where t is the time in day. The method is similar to that for constructing MJO based on the two leading EOFs of 850-hPa zonal wind (Maloney and Hartmann, 1998). Weakened convective anomalies associated with the center of positive correlations of OLR in the western

Pacific on day –4 (Fig. 5a) propagate eastward along the equator and reach the west coast of South America on day 4 (Fig. 5i). The associated upper-level convergent wind anomalies also move consistently eastward. During this 9-day period, the convective disturbances move from 160°E to 80°W across 120° in longitude, equivalent to a mean speed of 17 m s^{-1}.

The period of the convective disturbances can be estimated from Fig. 5. At the equator near 160°E, for example, the most inactive convection on day –4 becomes most active on day 0 (Fig. 5e) at the same location, indicating that the convective fluctuations have a period of 8 days. Similarly, the most active convection near 90°W on day 0 becomes most inactive on day 4,
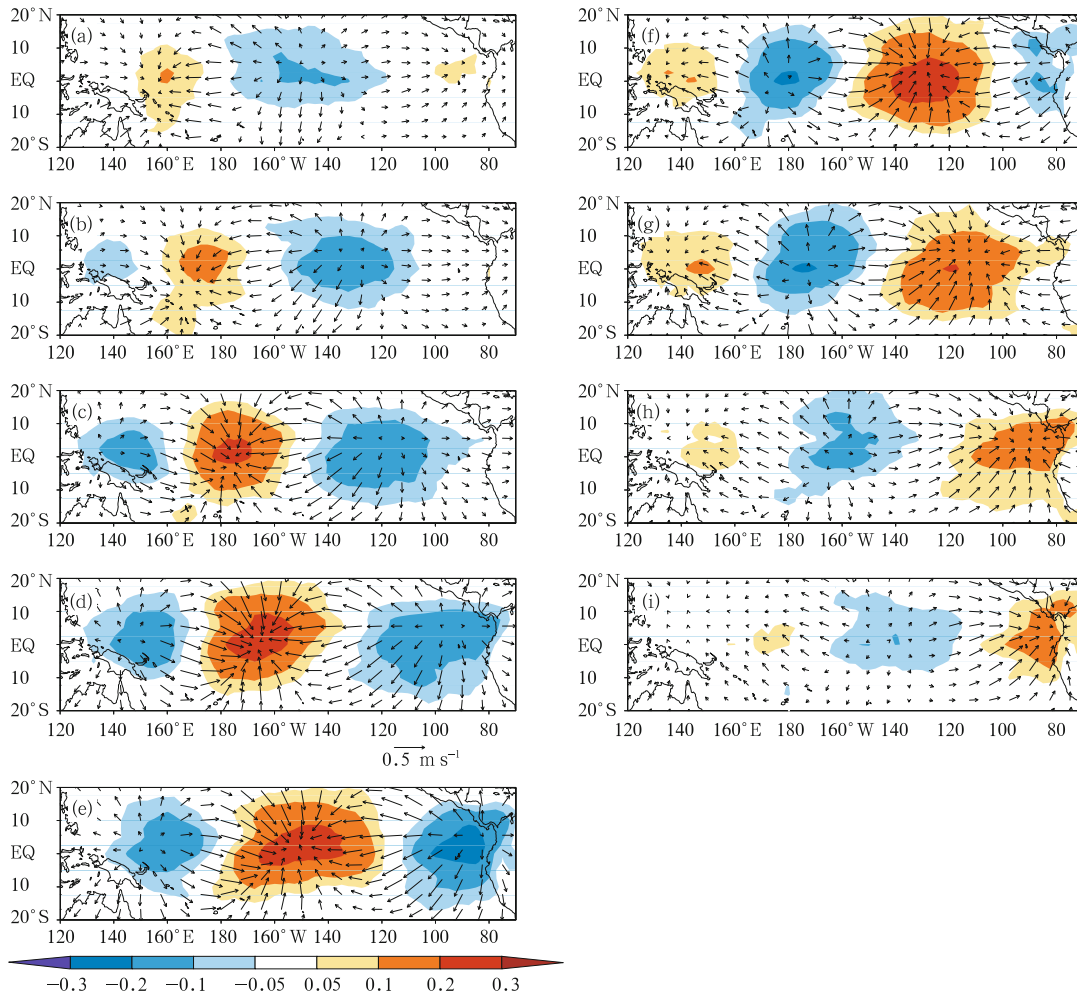
Fig. 5. Correlation maps of the filtered daily OLR (shadings) and regression maps of daily 200-hPa divergent wind (vectors; m s^{-1}) against the PC1 and PC2 time series for OLR and wind leading PC1 by (a) 4, (b) 3, (c) 2, (d) 1, and (e) 0 days, and lagging PC1 by (f) 1, (g) 2, (h) 3, and (i) 4 days. The spatial maps are constructed based on those associated with the two PC time series in the following manner: 0.5PC1+0.25[PC2(t+1)+PC2(t+2)].

also with a period of 8 days. The period estimated from Fig. 5 is consistent with that inferred from the lead and lag correlations between PC1 and PC2 in Fig. 3.

The convective disturbances with the period of 8 days, zonal wavenumber 3 or 4, and eastward-propagating phase speed of 17 m s^{-1} match the well-known Kelvin waves documented in Wheeler and Kiladis (1999) and Roundy and Frank (2004). The convective disturbances with such wave characteristics are identified as convectively coupled Kelvin waves above the 95% significance level in the wavenumber-frequency power spectrum of the OLR over the tropical Pacific (Straub and Kiladis, 2002).

The source of the convectively coupled Kelvin waves in the tropical Pacific can also be inferred from Fig. 5. On day –3, a small area of negative correlations of OLR is discernible in the western Pacific and becomes larger and moves eastward in the following days (day –2 to day 2). In the meantime, an upper-level outflow develops. This indicates that the anomalous convection associated with the Kelvin wave originates from the western Pacific. This is a part of the Indo-Pacific warm pool (e.g., Wang and Mehta, 2008) where SST is persistently higher than 301 K (28℃), a threshold for atmospheric deep convection (Fu et al., 1994). The results suggest that deep convection in the western Pacific warm pool may generate convectively coupled Kelvin waves, such as those represented by the pair of leading EOFs of ORL shown in Figs. 2 and 5, which propagate eastward across the tropical Pacific.

3.2 ENSO impact

How the underlying SST anomalies associated with ENSO affect the Kelvin wave activity is assessed for EP El Niño, CP El Niño, and La Niña, respectively. Figure 6 shows the composites of ENSO SST anomalies in December, January, and February, the peak phase of ENSO, for the 5 EP El Niño, 5 CP El Niño, and 8 La Niña events. Compared to the EP El Niño (Fig. 6a), the CP El Niño SST anomalies are weaker and cover a smaller area of the tropical Pacific (Fig. 6b). Both the amplitude and spatial coverage of the La Niña SST anomalies (Fig. 6c) are comparable to those of the EP El Niño.

Figures 7a and 7b display the seasonal distributions of the Kelvin wave activity associated with the two EOFs quantified by the monthly mean variance of normalized daily PC time series for each calendar month. The 30-yr mean Kelvin wave activity associated with both EOFs (black lines in Figs. 7a and 7b) is characterized by weak variability during August–December, increasing wave activity from January to March, and reaching peak values during April–June. The spread of the monthly mean wave activity over the 30 years (grey shading) is large for the Kelvin waves associated with EOF1 (Fig. 7a), especially during January–June, and relatively small associated with EOF2 (Fig. 7b).

During EP El Niños, SST is warmer in the central and eastern Pacific (Fig. 6a) and thus enhances local deep convection. Consistently, the monthly mean Kelvin wave activity averaged over the 5 EP El Niño years (red lines in Figs. 7a and 7b) is stronger than the 30-yr mean throughout the annual cycle. The enhancement of the wave activity is most significant during November–June for PC1 and October–January for PC2, with the increased variance greater than one standard deviation (1σ) of the 30-yr spreads. Compared to the 30-yr mean wave activity, the variance during the 5 EP El Niño is increased by 99% for PC1 and 63% for PC2, averaged over the 12 calendar months.

The impact of the CP El Niño on the Kelvin wave activity is much weaker (orange lines in Figs. 7a and 7b), due to much weaker SST anomalies and smaller areas covered by positive SST anomalies (Fig. 6b). In some months, such as January–July for PC1 and April–July for PC2, the intensity of the Kelvin waves even decreases. Overall, the changes (either increase or decrease) in the PC variance due to the CP El Niño are 19% and 17% of the 30-yr mean values for PC1 and PC2, respectively.

Associated with La Niña, the convectively coupled Kelvin wave activity is weakened coherently throughout all seasons (blue lines in Figs. 7a and 7b). However, the changes are within the range of 1σ of the 30-yr spreads, less significant than the changes associ-

ated with the EP El Niño. On average, the decreases in the PC variance are 33% and 24% of the 30-yr means for PC1 and PC2, respectively.

Although the La Niña SST anomalies are comparable to the EP El Niño SST anomalies in terms of amplitude and spatial coverage (Figs. 6a and 6c), their impact on the convectively coupled Kelvin wave activity is much weaker than that of the EP El Niño, that is, 33% vs. 99% for PC1 and 24% vs. 63% for PC2 with respect to the 30-yr mean variance. This indicates a nonlinearity of the Kelvin waves in response to ENSO SST anomalies. Because saturation vapor pressure is an exponential function of temperature, even a small

increase in SST, when SST is high, can significantly enhance the intensity of deep convection, as well as the associated wave activity. When SST is relatively low, deep convection and Kelvin waves are less sensitive to the change in SST. Additionally, there is also a saturation of mean precipitation in response to cold SST anomalies compared to warm anomalies (Hoerling et al., 1997). Changes in mean precipitation response may also reflect the changes in the sub-seasonal response of precipitation and convection to SST.

The modulations of the Kelvin wave activity by the different flavors of ENSO presented in Figs. 7a and 7b are only for those Kelvin waves depicted by
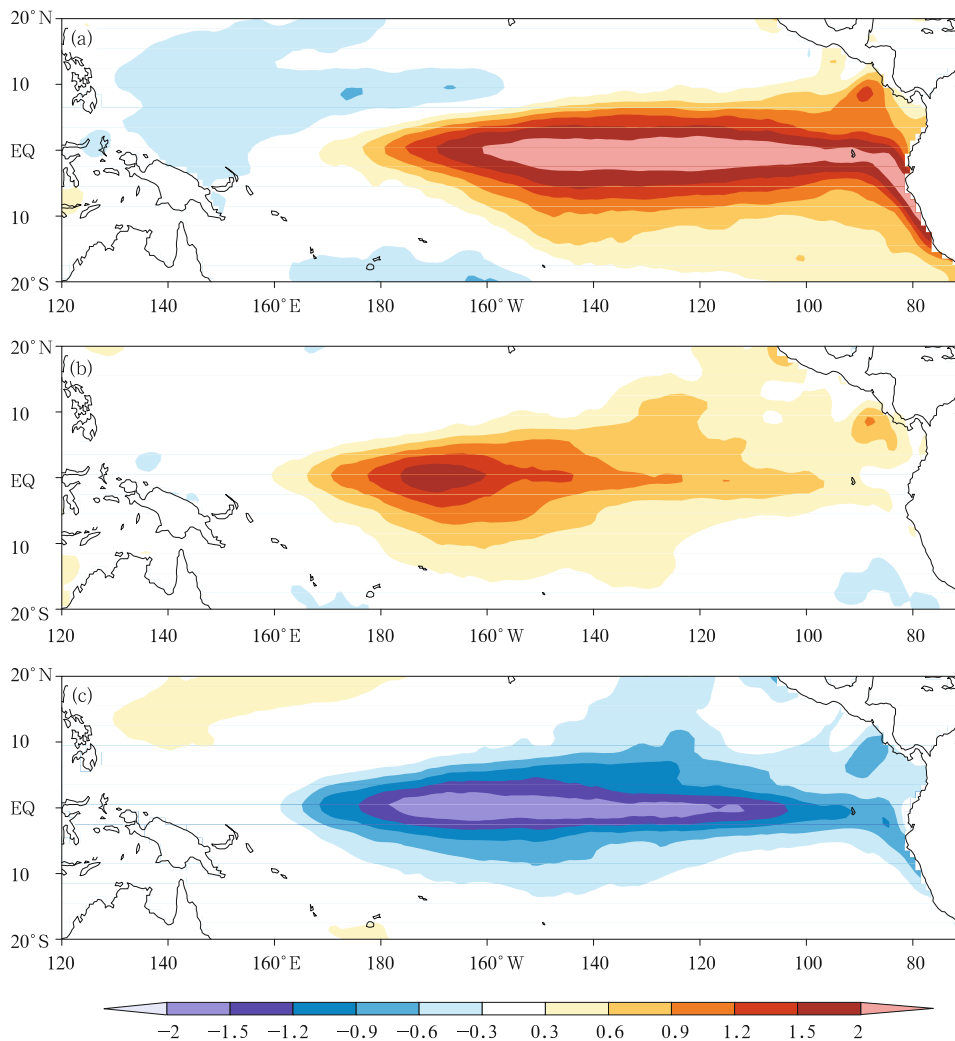
Fig. 6. Composites of December–January–February SST anomalies (K) for (a) EP El Niño (1982/83, 1986/87, 1991/92, 1997/98, and 2006/07), (b) CP El Niño (1987/88, 1994/95, 2002/03, 2004/05, and 2009/10), and (c) La Niña (1983/84, 1984/85, 1988/89, 1995/96, 1998/99, 1999/2000, 2005/06, and 2007/08).
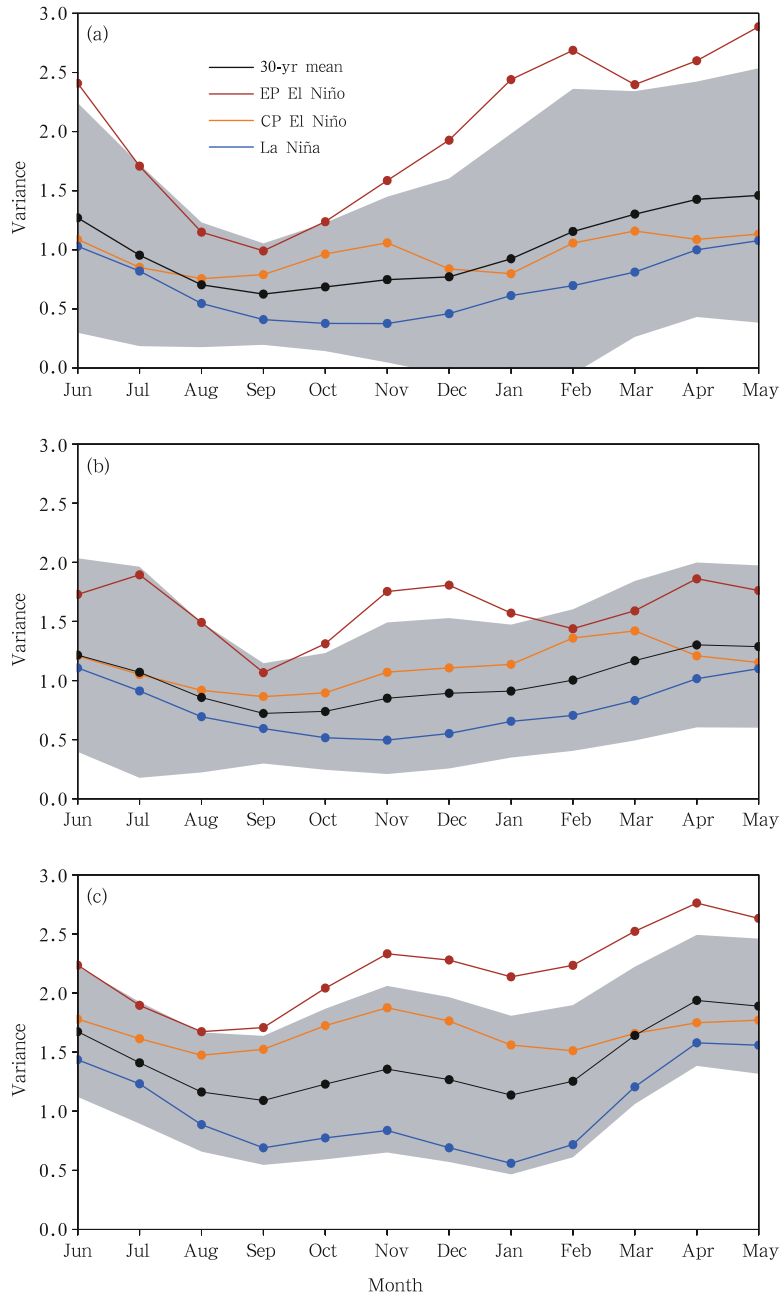
Fig. 7. Seasonal distributions of monthly mean variance of daily (a) PC1 and (b) PC2 time series and (c) monthly mean variance ($W^2\ m^{-4}$) of band-pass (2–25-day) filtered daily OLR averaged over the tropical Pacific (10°S–10°N, 160°E–80°W) for the entire 30 years (black), 5 EP El Niño years (red), 5 CP El Niño years (orange), and 8 La Niña years (blue). Grey shadings denote the range of ±1σ of the 30-yr spreads around the 30-yr mean variance.

the pair of leading EOFs (Fig. 2) with specific wavelength. The conclusions drawn from Figs. 7a and 7b thus may not be true for other Kelvin waves with different spatial characteristics. To address this concern, Fig. 7c shows the seasonal distribution of monthly mean variance of the band-pass (2–25-day) filtered daily OLR averaged over the tropical Pacific (10°S–10°N, 160°E–80°W) for the entire 30 years, as well as different ENSO categories. Overall, the modulations of the sub-monthly convective activities by the different ENSO flavors are in agreement with those of the Kelvin waves with specific wavelength discussed here

(Figs. 7a and 7b). In Fig. 7c, the impact of EP El Niño (red line) is still largest. The impacts of CP El Niño (orange line) and La Niña (blue line) are also within 1σ of the 30-yr spreads (grey shading). However, the latter two are larger as compared to their counterparts for the Kelvin waves in Figs. 7a and 7b.

The modulation of the convectively coupled Kelvin waves by ENSO is also assessed through the power spectrum analysis. Figure 8 presents the power spectra of 365-day PC time series (1 June of a year to 31 May of the following year) averaged over the 30-yr period (black lines), 5 EP El Niño years (red lines), 5 CP El Niño years (orange lines), and 8 La Niña years (blue lines), respectively, for PC1 and PC2. In addition to the period of 8 days estimated from Figs. 3 and 5, the 30-yr mean power spectra display significant peaks over the 5–20-day window.

Associated with the EP El Niño, the power is dramatically increased over almost the entire 5–20-day window for both PCs. Associated with the CP El Niño, in contrast, the power is enhanced only at some periods, for example, at 7 and 9 days for PC1 and between 16 and 20 days for PC2. The power is generally decreased in La Niña years. The results indicate that the convectively coupled Kelvin waves are largely intensified by the EP El Niño, less affected by the CP El Niño, and slightly weakened by La Niña. Additionally, there are also shifts of the peaks associated with different ENSO flavors in the power spectra, suggesting possible modulations of the frequency of the Kelvin waves by ENSO.

To further assess the modulation of the Kelvin waves by ENSO, we look at the lagged correlations between filtered daily OLR and the two PCs in the 5 EP El Niño years and 8 La Niña years, respectively, for OLR leading PC1 4 days (day –4) to 1 day (day –1) shown in Fig. 9. The spatial patterns are constructed based on the two EOFs in the same way as for Fig. 5. The negative correlations are stronger (weaker) over the central and eastern Pacific (the western Pacific) during EP El Niño than those during La Niña, indicating stronger convection over warmer SST.

Compared to the mean wave structure over the 30 years (Fig. 5, left panels), the Kelvin waves associ-

ated with the EP El Niño have slightly shorter wavelengths and propagate eastward a little more slowly (about 15 m s^{-1}). This is consistent with the finding of Roundy (2012) that the Kelvin waves tend to move eastward more slowly over warmer water. It can also be explained by the reduction of effective static stability due to condensational heating (e.g., Wang and Li, 1994). In the La Niña years, they have slightly longer wavelengths and move eastward a little faster (about 20 m s^{-1}). Overall, the changes in wavelength and phase speed due to ENSO are about 10%–20% of the 30-yr means, and less significant than the change in the intensity of the Kelvin waves.

4. Summary

We have investigated the influence of ENSO on the characteristics of the convectively coupled Kelvin waves over the tropical Pacific based on the comparisons of the Kelvin wave activity in the EP El Niño,
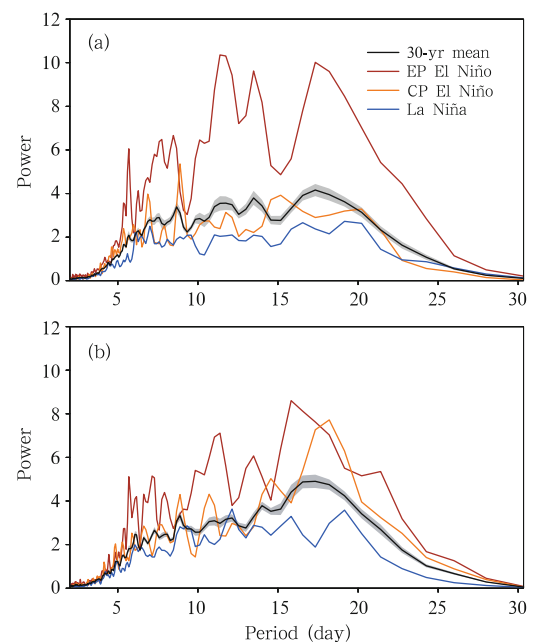
Fig. 8. Power spectra of the 365-day (a) PC1 and (b) PC2 time series for 30-yr mean (black), 5-yr mean EP El Niño (red), 5-yr mean CP El Niño (orange), and 8-yr mean La Niña (blue). Grey shadings denote the 95% uncertainty range of the 30-yr mean spectra based on the Jackknife estimate.
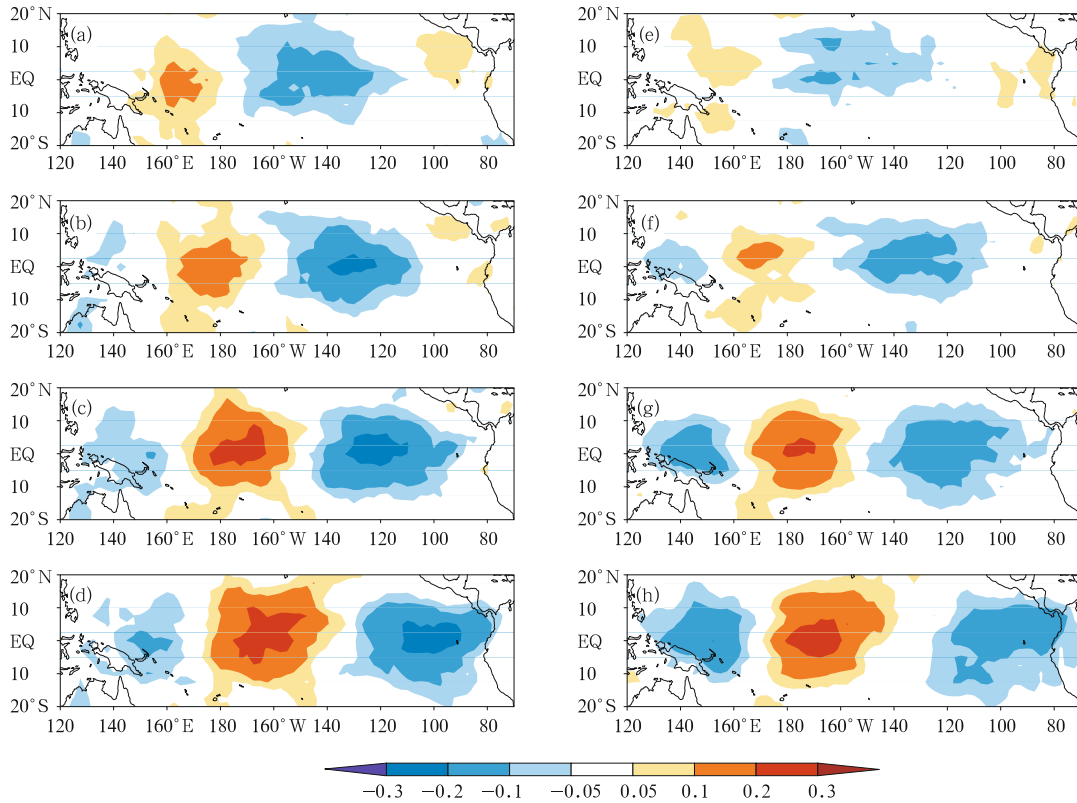
Fig. 9. Correlation maps of filtered daily OLR with the PC1 and PC2 time series for OLR leading PC1 by (a, e) 4, (b, f) 3, (c, g) 2, and (d, h) 1 days over 5 EP El Niño years (left panels) and 8 La Niña years (right panels), respectively. The spatial maps are constructed based on those associated with the two PC time series in the following manner: $0.5PC1+0.25[PC2(t+1)+PC2(t+2)]$.

CP El Niño, and La Niña years. The convectively coupled Kelvin waves in this study are represented by the two leading EOFs of filtered daily OLR anomalies, with the estimated zonal wavenumber of 3 or 4, period of 8 days, and eastward propagating speed of about 17 m s^{-1}. The most significant impact of ENSO on the Kelvin wave activity is the remarkable intensification of the Kelvin waves during the EP El Niño. The impact of La Niña on the reduction of the Kelvin wave intensity is relatively weak, reflecting the nonlinearity of tropical deep convection and the associated Kelvin waves in response to the ENSO SST anomalies. The impact of the CP El Niño on the Kelvin waves is less significant. In addition, ENSO may alter the frequency, wavelength, and phase speed of the Kelvin waves on a marginal to moderate scale.

It is noted that convectively coupled Kelvin waves have a broad range of spatial scales from zonal wavenumber 2 to 10 (e.g., Wheeler and Kiladis, 1999). The Kelvin waves depicted by the pair of leading EOFs in Fig. 2 represent only a fraction of the equatorially-trapped Kelvin waves, indicating the limitation of this approach in extracting the Kelvin waves. Additionally, the time-filtered OLR data used in this study contain not only eastward moving convection but also westward moving convection, both of which may project onto the two EOF patterns. Furthermore, extratropical atmospheric waves with different wave characteristics may intrude into the tropics and generate the Kelvin wave-like disturbances (e.g., Straub and Kiladis, 2003a), which could alter the spectral peaks of pure Kelvin waves. These deficiencies could be avoided with the more sophisticated space-time filter (Wheeler and Kiladis, 1999) for the Kelvin waves.

There are several other aspects that could also be the topics of our future work. We explored the ENSO

impact on the wave characteristics of the convectively coupled Kelvin waves. The impact may also extend to the vertical structure of the dynamical fields associated with the Kelvin waves (Wheeler et al., 2000; Straub and Kiladis, 2003b). Besides the tropical Pacific, convectively coupled Kelvin waves over the tropical Indian Ocean (Roundy, 2008) and the tropical Atlantic (Wang and Fu, 2007) may also be modulated by ENSO through atmospheric teleconnection and local air-sea interaction.

This study illustrated the modulation of synoptic-scale and high-frequency wave activity by the low-frequency SST variations, an example of weather-climate linkage. On the other hand, the Kelvin wave may not only respond but also feedback to the SST anomalies. For example, surface westerly wind bursts are known to play an important role in triggering the 1997/98 El Niño (McPhaden, 1999). Strong surface westerly wind anomalies do exist following the anomalous deep convection associated with the Kelvin waves (e.g., Straub and Kiladis, 2002; Wang and Fu, 2007). How the wind anomalies associated with the Kelvin waves might affect SST could be an interesting topic for future work.

REFERENCES

Ashok, K., S. K. Behera, S. A. Rao, et al., 2007: El Niño Modoki and its possible teleconnection. *J. Geophys. Res.*, **112**, C11007, doi: 10.1029/2006JC003798.

Dias, J., and O. Pauluis, 2011: Modulations of the phase speed of convectively coupled Kelvin waves by the ITCZ. *J. Atmos. Sci.*, **68**(7), 1446–1459.

Duchon, C. E., 1979: Lanczos filter in one and two dimensions. *J. Appl. Meteor.*, **18**(8), 1016–1022.

Fu, R., A. D. Del Genio, and W. B. Rossow, 1994: Influence of ocean surface conditions on atmospheric vertical thermodynamic structure and deep convection. *J. Climate*, **7**(7), 1092–1108.

Hoerling, M. P., A. Kumar, and M. Zhong, 1997: El Niño, La Niña, and the nonlinearity of their teleconnections. *J. Climate*, **10**(8), 1769–1786.

Kanamitsu, M., W. Ebisuzaki, J. Woollen, et al., 2002: NCEP-DOE AMIP-II reanalysis (R-2). *Bull. Amer. Meteor. Soc.*, **83**(11), 1631–1643.

Kao, H. -Y., and J.- Y. Yu, 2009: Contrasting eastern-Pacific and central-Pacific types of ENSO. *J. Climate*, **22**(3), 615–632.

Kim, S. T., and J. -Y. Yu, 2012: The two types of ENSO in CMIP5 models. *Geophys. Res. Lett.*, **39**, L11704, doi: 10.1029/2012GL052006.

Laing, A. G., R. E. Carbone, and V. Levizzani, 2011: Cycles and propagation of deep convection over equatorial Africa. *Mon. Wea. Rev.*, **139**(9), 2832–2853.

Liebmann, B., and C. A. Smith, 1996: Description of a complete (interpolated) outgoing longwave radiation dataset. *Bull. Amer. Meteor. Soc.*, **77**(6), 1275–1277.

——, G. N. Kiladis, L. M. V. Carvalho, et al., 2009: Origin of convectively coupled Kelvin waves over South America. *J. Climate*, **22**(2), 300–315.

Maloney, E. D., and D. L. Hartmann, 1998: Frictional moisture convergence in a composite life cycle of the Madden-Julian oscillation. *J. Climate*, **11**(9), 2387–2403.

McPhaden, M. J., 1999: Genesis and evolution of the 1997–98 El Niño. *Science*, **283**(5404), 950–954.

Mounier, F., S. Janicot, and G. N. Kiladis, 2008: The West African monsoon dynamics. Part III: The quasi-biweekly zonal dipole. *J. Climate*, **21**(9), 1911–1928.

Neelin, J. D., F. -F., Jin, and H.- H. Syu, 2000: Variations in ENSO phase locking. *J. Climate*, **13**(14), 2570–2590.

North, G. R., T. L. Bell, R. F. Cahalan, et al., 1982: Sampling errors in the estimation of empirical orthogonal functions. *Mon. Wea. Rev.*, **110**(7), 699–706.

Reynolds, R. W., N. A. Rayner, T. M. Smith, et al., 2002: An improved in situ and satellite SST analysis for climate. *J. Climate*, **15**(13), 1609–1625.

Roundy, P. E., 2008: Analysis of convectively coupled Kelvin waves in the Indian Ocean MJO. *J. Atmos. Sci.*, **65**(4), 1342–1358.

——, 2012: The spectrum of convectively coupled Kelvin waves and the Madden-Julian oscillation in regions of low-level easterly and westerly background flow. *J. Atmos. Sci.*, **69**(7), 2107–2111.

——, and W. M. Frank, 2004: A climatology of waves in the equatorial region. *J. Atmos. Sci.*, **61**(17), 2105–2132.

Straub, K. H., and G. N. Kiladis, 2002: Observations of a convectively coupled Kelvin wave in the eastern Pacific ITCZ. *J. Atmos. Sci.*, **59**(1), 30–53.

——, and ——, 2003a: Extratropical forcing of convectively coupled Kelvin waves during austral winter. *J. Atmos. Sci.*, **60**(3), 526–543.

——, and ——, 2003b: The observed structure of convectively coupled Kelvin waves: Comparison with simple models of coupled wave instability. *J. Atmos. Sci.*, **60**(14), 1655–1668.

Wang, B., and T. M. Li, 1994: Convective interaction with boundary-layer dynamics in the development of a tropical intraseasonal system. *J. Atmos. Sci.*, **51**(11), 1386–1400.

Wang, H., and R. Fu, 2007: The influence of Amazon rainfall on the Atlantic ITCZ through convectively coupled Kelvin waves. *J. Climate*, **20**(7), 1188–1201.

——, and V. M. Mehta, 2008: Decadal variability of the Indo-Pacific Warm Pool and its association with atmospheric and oceanic variability in the NCEP-NCAR and SODA reanalyses. *J. Climate*, **21**(21), 5545–5565.

——, A. Kumar, W. Q. Wang, et al., 2012: U.S. summer precipitation and temperature patterns following the peak phase of El Niño. *J. Climate*, **25**(20), 7204–7215.

Wheeler, M., and G. N. Kiladis, 1999: Convectively coupled equatorial waves: Analysis of clouds and temperature in the wavenumber-frequency domain. *J. Atmos. Sci.*, **56**(3), 374–399.

——, ——, and P. J. Webster, 2000: Large-scale dynamical fields associated with convectively coupled equatorial waves. *J. Atmos. Sci.*, **57**(5), 613–640.

Wilks, D. S., 1995: *Statistical Methods in the Atmospheric Sciences.* Academic Press, London, 467 pp.

Yeh, S. -W., J. -S. Kug, B. Dewitte, et al., 2009: El Niño in a changing climate. *Nature*, **461**(7263), 511–514.